ADVANCED MATERIALS TECHNOLOGIES
www.advmattechnol.de

A Field-Deployable, Wearable Leaf Sensor for Continuous Monitoring of Vapor-Pressure Deficit

*Shihao Yin, Hussam Ibrahim, Patrick S. Schnable, Michael J. Castellano, and Liang Dong**

This work presents a wearable sensor for real-time on-leaf monitoring of relative humidity (RH), temperature, and vapor-pressure deficit (VPD) of plants in both controlled environments and under field conditions. This sensor is flexible and conformable to the leaf surface. By integrating a graphene-based RH sensing element and a gold-based thin-film thermistor on a polyimide sheet, the sensor allows accurate and continuous determination of VPD at the leaf surface, thereby providing information on plant transpiration. A greenhouse experiment validates the ability of the sensor to continuously and simultaneously monitor both the leaf RH and temperature of maize plants over more than 2 weeks. The sensor output also demonstrates the influences of light and irrigation on maize transpiration. Uniquely, by attaching multiple sensors onto different locations of a plant, it is possible to estimate the time required for water to be transported from the roots to each of the measured leaves along the stalk, as well as longitudinally from one position on a leaf toward the leaf tip. Sensors are also deployed in crop production fields where they demonstrate the ability to detect difference in transpiration between fertilized and unfertilized maize plants.

1. Introduction

Plants use stomata, small openable pores on the undersides of their leaves to uptake the carbon dioxide required for photosynthesis. Environmental factors, such as temperature,[1] relative humidity (RH),[2] light,[3] and soil water availability[4] regulate the opening and closing of stomata. When stomata are open they release water vapor via a process termed "transpiration".[5] Transpiration not only cools the plants, but also affects nutrient uptake, photosynthesis, and the transport of water within the plant-soil system. Within and across plant species, genetic and physiological factors contribute to the function of stomata, ultimately impacting nutrient and water use efficiencies (i.e., the exchange of carbon dioxide and oxygen, the uptake of nutrients per unit of water transpiration) particularly under drought.[6]

Vapor-pressure deficit (VPD) is the driving force of transpiration and there are strong positive relationships between VPD and plant transpiration rate.[7] Essentially, VPD describes the difference between the theoretical pressure exerted by water vapor held in saturated air at a given temperature, and the pressure exerted by the water vapor that is actually held in the air at the same temperature. Therefore, VPD takes account of temperature and RH both at the leaf surface and in the air. VPD can be too high or low for optimum plant growth. High VPD indicates a dry growth environment such that plants must use more water to acquire a given amount of carbon dioxide.[8] Drought stress occurs when the transpiration rate exceeds the rate that at which water can translocate from the roots to the leaves.[9,10] Alternatively, at low VPD, leaf surfaces become saturated and disease and fungal growth become the concerns.[11] The decrease in the water flowing inside the plant also causes the difficulty for the nutrient to be assimilated from the root and transported to other parts, as well as the assimilates from leaves to the rest of the plant. Therefore, frequent and accurate monitoring of VPD will allow farmers to manage growth environments for optimum water and nutrient use efficiencies while potentially improving disease control. However, VPD estimation based on monitoring of air RH and temperature is not optimal due to the lack of the information on RH and temperature at leaf surfaces. The VPD at the leaf surface can be very different from the surrounding air. There have been considerable efforts to improve the accuracy of VPD estimation using sensors and imaging technologies.[12] Temperature and RH sensors with a small factor form are widely available[13,14]; they, however, are often not sufficiently flexible and low-mass for direct installation on leaf surfaces; on-leaf installation of current sensors requires a complex, heavy, and large assembly.[15] While infrared imaging-based thermometers allow direct measurement of leaf surface temperature,[16] it still remains challenging to use this technology in long-term and large-scale VPD measurement.

Low-cost sensors for monitoring of RH and temperature (hence VPD) on the leaf are still in their infancy. However, flexible RH and temperature sensors have been developed for a variety of emerging applications.[17–22] Our group initiated a wearable plant sensor using a graphene-based water vapor-sensitive material for

S. Yin, H. Ibrahim, Prof. L. Dong
Department of Electrical and Computer Engineering
2520 Osborn Dr, Ames, IA 50011, USA
E-mail: ldong@iastate.edu
Prof. P. S. Schnable, Prof. M. J. Castellano
Agronomy Department
Iowa State University
2520 Osborn Dr, Ames, IA 50011, USA
The ORCID identification number(s) for the author(s) of this article can be found under https://doi.org/10.1002/admt.202001246.

DOI: 10.1002/admt.202001246

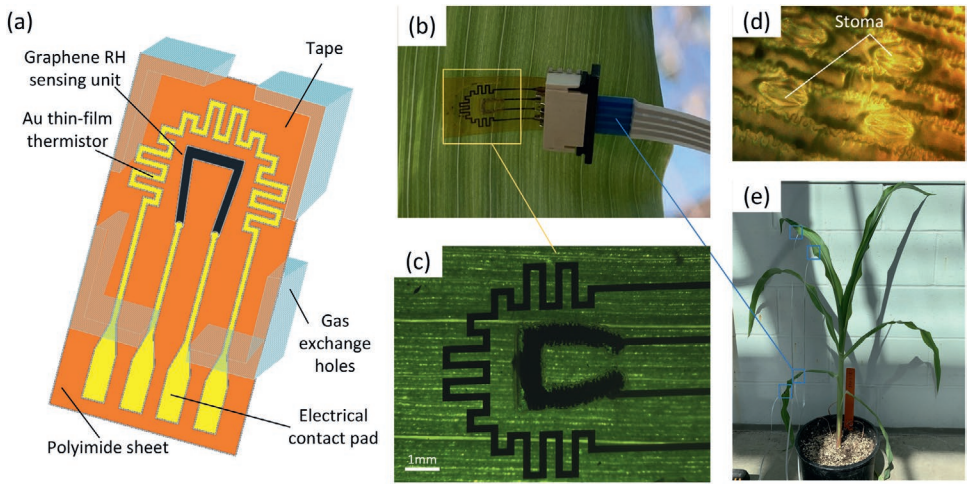

Figure 1. a) Schematic of the integrated temperature and humidity sensor formed on a flexible substrate. The sensor consists of a gold thin-film-based temperature sensor and a laser-induced graphene-based RH sensor. b) Sensor installation on the leaf. c) Close-up of the installed leaf sensor. d) Microscope image of stomata on the back of leaf surface. e) A maize plant with two sensors installed on a lower leaf and two sensors on the upper leaf. This sensor system allows monitoring the vertical water transport along the stalk and lateral water transport from one area (close to the stem) to another (far away from the stem) in the leaf.

direct monitoring of RH changes on the leaf surface.[23] Recently, graphene-based capacitive humidity sensors have also demonstrated rapid responses to RH changes.[24] Another recently developed flexible sensor has been reported for monitoring illumination, RH, and temperature on the leaf.[25] Despite the development of several plant sensors,[26–31] existing on-leaf RH and temperature sensors are limited to measurements in the greenhouse over relatively short periods of time; the performances of these sensors under field conditions have not been studied.

In this paper, we report the development of a wearable leaf sensor for real-time monitoring of RH and temperature for accurate determination of VPD at the leaf surface (**Figure 1**a,b). This sensor is flexible and conformable to the leaf surface. The device uses a flexible polyimide sheet as the substrate, laser-induced graphene (LIG) flakes for RH measurement, and a gold (Au)-based thin-film thermistor for temperature measurement (Figure 1c). On-demand formation and patterning of LIG are realized by direct laser writing on the polyimide sheet. The irradiation power and moving speed of the laser beam are optimized. It is demonstrated that the patterned LIG exhibits a rapid response to transpiration-induced RH changes, which, in conjunction with the integrated thermistor, enables continuous VPD monitoring on the leaf. We demonstrate in the greenhouse that the leaf sensors can continuously monitor variations in leaf RH and temperature for more than 2 weeks under different light and irrigation conditions. Further, by incorporating multiple sensors on multiple leaves of a plant that differ in distance from the plant roots, we quantify differences in transpiration between these leaves (Figure 1e). This provides a new ability to quantify the time required for water movement within a plant from the roots to each of the measured leaves. Moreover, for the first time, we deployed the wearable VPD sensor in crop fields. Our pilot experiment has validated that the sensor can differentiate transpiration of fertilized and unfertilized corn plants. The measurement results herein represent the most detailed temporal resolution information on plant transpiration at the leaf surface to date.

2. Design and Fabrication

Generally, VPD is estimated by $\mathrm{VPD} = \mathrm{VP_{sat}} - \mathrm{VP_{air}}$. $\mathrm{VP_{sat}}$ represents the saturated vapor pressure inside a leaf and is given by $\mathrm{VP_{sat}} = 0.6107 \times 10^{7.5T_l/(273.3+T_l)}$, where T_l is the temperature on the leaf in Celsius. $\mathrm{VP_{air}}$ is the air vapor pressure and is given by $\mathrm{VP_{air}} = 0.6107 \times 10^{7.5T_a/(273.3+T_a)} \times \mathrm{RH}/100$, where T_a is the air temperature in Celsius, and RH is the relative humidity at the leaf surface.[32] Therefore, accessing accurate information on the leaf temperature and RH and the air temperature will allow accurate estimation of VPD. In the present sensor, a LIG-based resistive RH sensing unit and an Au-based thin-film thermistor are integrated on a 100 µm-thick polyimide sheet. To attach the sensor to the surface of leaf, a 1 mm-thick waterproof double-sided adhesive is applied on the edges of the polyimide sheet. This also creates a thin air gap between the leaf surface and the sensor. To minimize the disturbance of the sensor to the plant growth during long-term monitoring, several openings are formed in the tape as breathing holes for enabling sufficient exchange of water vapor, carbon oxide, and oxygen between the leaf and atmosphere during the plant growth. When water molecules exit the stomata (Figure 1d), the RH level at the leaf surface increases, leading to an increase in the electrical resistance of the patterned LIG. Essentially, due to the application of photothermal energy during direct laser writing, the sp3-carbon atoms in the polyimide sheet are converted to sp2-carbon atoms, rendering the obtained LIG with a similar chemical and structural feature to reduced graphene oxide that is sensitive to water vapor.[33] Thin-film Au is chosen as the thermistor material because its resistance changes with temperature with a temperature coefficient of resistance TCR = 0.0034 per°C.[34] To obtain the output signal from the sensor by using external electronics, the contact pads of the sensor are connected with an electronic wire connector and firmed with waterproof epoxy. Due to the light weight and flexibility of the sensor, it is able to conformably attach to the leaf surface.

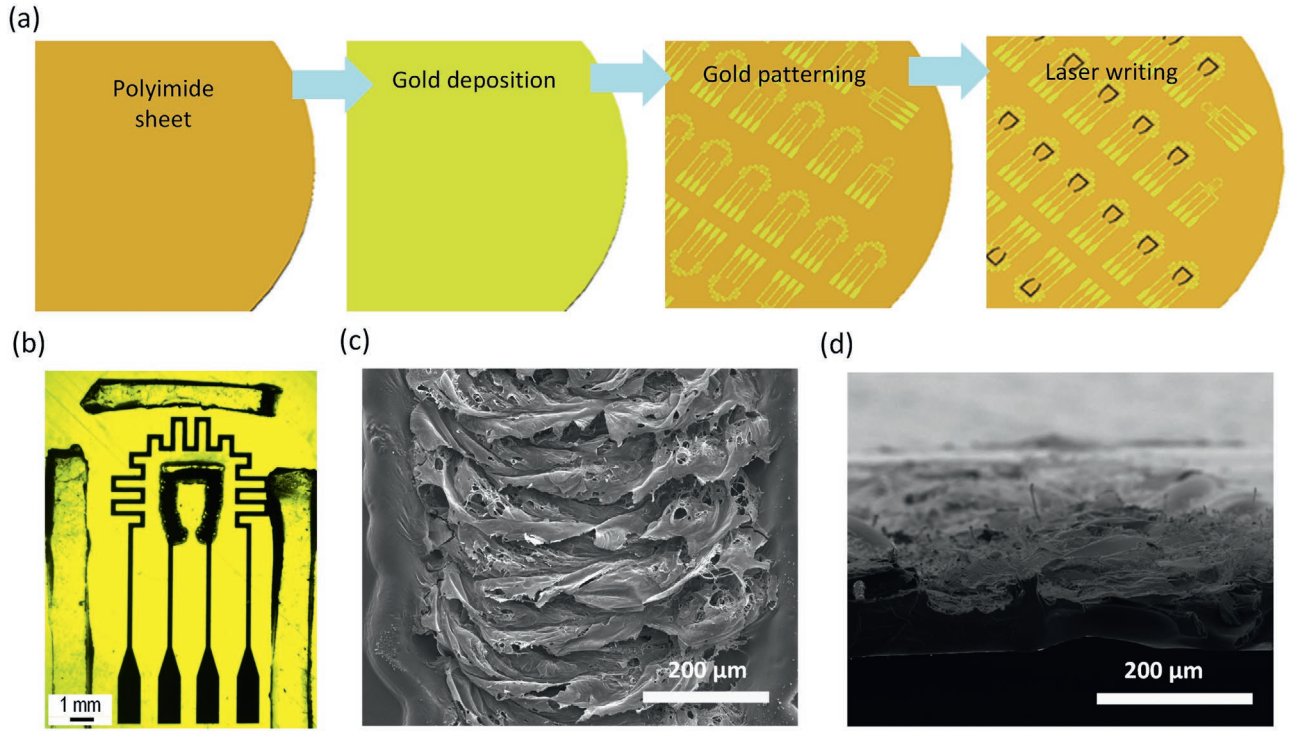

Figure 2. a) Schematic of the fabrication process flow for the present sensor. b) Top view of the integrated temperature and RH sensor. The sensors are surrounded by double-sided tape with breathing holes for gas exchange. c) SEM perspective image of LIG. d) SEM cross-sectional view of LIG.

To fabricate the sensor on the polyimide sheet (**Figure 2**a,b), the sheet was first attached to a silicon wafer with double-sided tape. Then, a 5 nm-thick titanium layer and a 200 nm-thick Au layer were sequentially deposited on the polyimide sheet substrate by e-beam evaporation. Next, conventional photolithography was applied to form serpentine patterns of a thin-film Au thermistor. To realize LIG-based RH sensing units units (Figure 2c,d), a laser writing method was applied to form LIG patterns on the polyimide sheet by using a laser cutting machine (Kehui K40 CO2 laser engraver; maximum power: 40 W). As described later, the processing conditions of the laser writing were optimized to be the irradiation power of 3.3 W and the moving speed of 10 mm s^{-1}, to avoid direct ablation of the polyimide sheet and compromise between high conductivity and patterning resolution.

3. Results and Discussion

3.1. Material and Device Characterizations

Various LIG patterns were formed through the laser-inducement method with the optimal resolution of ≈0.1 mm (**Figure 3**a–c). Multiple combinations of the irradiation power and moving speed were tested to obtain high conductivity and patterning resolution. The moving speed of the laser head was controlled in the range from 1 to 50 mm s^{-1}, while the irradiation power was adjusted between 3 to 4 W. When the moving speed increased to 50 mm s^{-1}, it was hard to obtain clear LIG patterns due to the insufficient irradiation power (Figure 3d). When the power was set below 3 W, no clear LIG patterns were observed on the polyimide sheet either. With increasing power to 4 W, the polyimide sheet was ablated, leaving holes through the thickness of the sheet (Figure 3e).

To examine the influence of the irradiation power on the structural properties of LIG, Raman spectroscopy (wavelength: 532 nm; power: 7.08 mW; integration time: 4 s) was used to analyze the LIG samples formed with different laser powers of 3.1, 3.3 and 3.5 W. The Raman spectra (Figure 3g) show that these samples exhibit almost the same peak wavelengths, including the D band peak of ≈1350 cm^{-1}, the G band peak at ≈1580 cm^{-1}, and the 2D band at ≈2700 cm^{-1}. These peak wavelengths are compatible with literature concerned with Raman evidence linking properties and structures.[35–38] Essentially, the origin of the D mode in LIG is associated with the defect-induced double-resonant scattering, while the D band peak is caused by the intervalley scattering process. Thus, the appearance and increase in intensity of the D band are evident in the introduction of structural defects in the graphene layer. In addition, X-ray photoelectron spectroscopy (XPS) analysis was conducted for the LIG samples (Figure 3h). There was supposed to be separation between C—C and C=C peaks; however, probably due to the insufficient resolution of the spectrometer, only a single signal is present in the XPS spectra and compared with the peaks corresponding to the carbon atoms bounded with other groups. The C1s peak of the LIG indicates the degree of oxidation and the presence of different oxygen functional groups in the LIG. The XPS spectra of these samples are found to be little changed with varying laser power applied. The result shows that the laser power has few influences on the performance of the formed LIG.

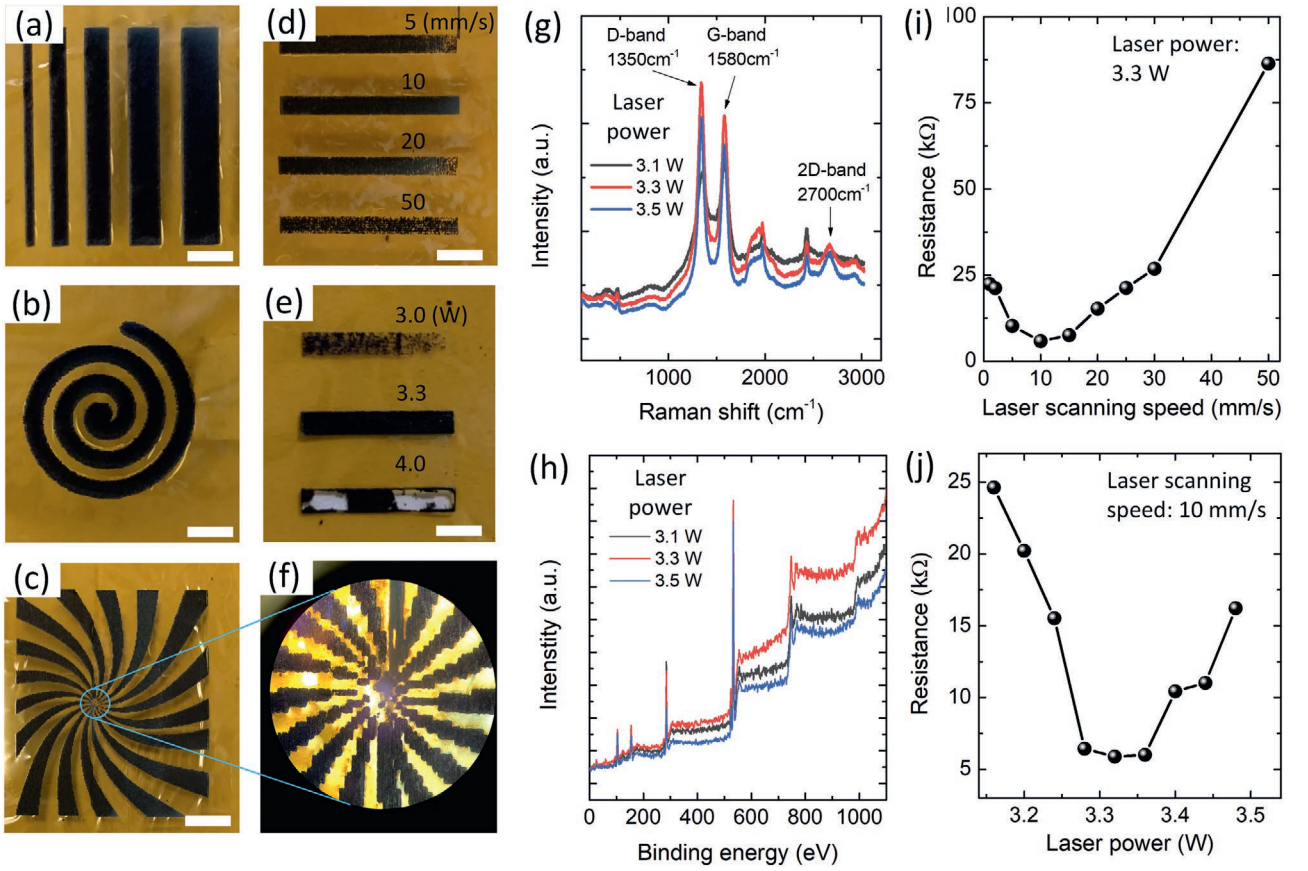

Figure 3. a–c) Optical images of various LIG patterns. d) LIG patterns formed with different moving speeds of the laser, given the irradiation power at 3.3 W. e) LIG patterns formed with different laser powers, given the same laser speed at 10 mm s^{-1}. f) Microscopic image of the center of (c). g) Raman and h) XPS spectroscopy of the LIG samples formed with the laser power at 3.1, 3.3, and 3.5 W. i,j) Electrical resistance as a function of moving speed (i) and power (j) of the laser. The scale bars in (a–e) represent 1 mm.

Figure 3i shows that given a laser power, as the moving speed of the laser increases, the resistance of the LIG reduces until reaching a minimum resistance of ≈5.8 kΩ at 10 mm s^{-1}; with increasing the moving speed further, the LIG pattern becomes less clear and its resistance increases (e.g., 86.4 kΩ at 50 mm s^{-1}). **Figure 4**d shows that at the 10 mm s^{-1} moving speed, with increasing irradiation power from 3 to 4 W, the resistance of the samples first reduces due to the formation of graphite and then increases for the formation of cracks at high power. At 4 W, the LIG becomes mechanically weak and is easily detached from the polyimide sheet (here, the attachment evaluation was performed by applying Scotch tape to and then peeling from the LIG samples). The LIG exhibits the minimum resistance of ≈5.8 kΩ at 3.3 W, while remaining strong attachment to the polyimide substrate. Therefore, when the laser power is too low and the speed is too high, the LIG pattern will not be well formed with a high resistance; when the power is too high and the speed is too low, the polyimide sheet will burn or cracks will form. Therefore, we chose the 10 mm s^{-1} moving speed and 3.3 W irradiation power to fabricate the LIG-based RH sensing unit.

The integrated sensor was characterized in a testing chamber where the internal RH and temperature could be controlled. Figure 4a shows that the LIG-based RH sensor exhibits an increase in resistance with increasing RH. The sensitivity of the LIG sensor is found to be ≈0.042 and ≈0.104 (relative resistance change per 1% change in RH) in the RH range from 25% to 75%, and from 75% to 100%, respectively (Figure 4a). The response time of the LIG sensor to a change in RH is ≈10 s, comparable to other LIG-based RH sensors reported.[39–42] Figure 4b shows the response of the fabricated Au-based thermistor to temperature variations. The thermistor provides an initial resistance of ≈28.6 Ω at room temperature (25 °C), and exhibits a linear response to temperature changes from 5 to 45 °C with the sensitivity of ≈0.23% per °C. It should be noted that the resistance change of the LIG sensor is negligible, even when the temperature increases from 5 to 45 °C; the Au-based thermistor sensor is also found insensitive to changes in environmental RH from 25% to 100%.

3.2. Plant VPD Measurements

The validation of the sensor in the greenhouse involved installing the fabricated sensors on different leaves of maize plants (growth stage at the time of sensor installation: 9th-leaf stage; genotype: B73). The sensors were attached to the back of the leaves. The leaf temperature and RH were monitored

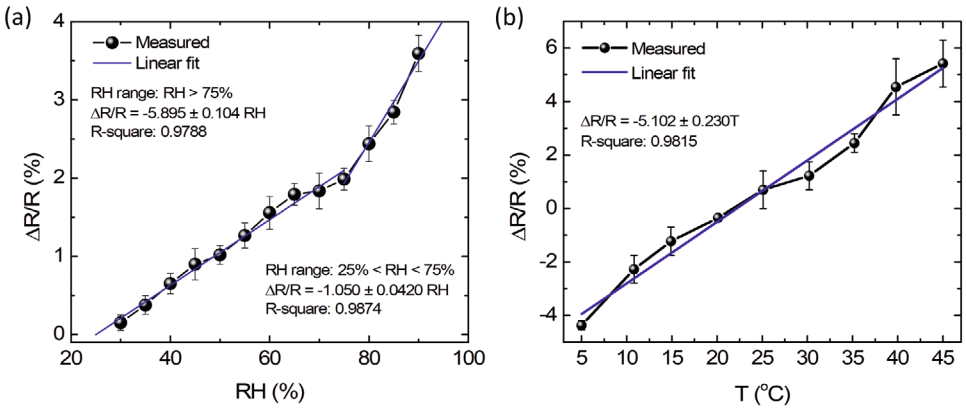

Figure 4. a) Relative change in resistance of the LIG-based RH sensing unit responding to changing environmental RH in a test chamber. b) Relative change in resistance of the Au-based thin-film thermistor responding to changing environmental temperature in the test chamber. The RH and temperature were obtained from a commercial RH and temperature sensor (SHT11, SENSIRION) placed inside the chamber.

over 16 days (from the 22nd of April to the 8th of May 2020). The values of VPD were calculated based on the measured RH and temperature. The air RH and temperature and light illumination in the greenhouse were controlled by a central control system. The growth light in the greenhouse was switched ON at 6 a.m. and OFF at 9 p.m. every day; however, there still occurred interference from the natural light outside the greenhouse. Multiple irrigations were scheduled in the course of the experiment. Data loggers were used to record the resistance changes of the sensors at a sampling rate of once per minute.

It should be noted that although the genotype (B73) and growth condition of the maize plants are the same, there appear plant-to-plant variations in growth, development, and response to the same agricultural management practices (e.g., fertigation and irrigation). Therefore, a statistical analysis was performed based on the data obtained from monitoring multiple plants. **Figure 5**a gives the mean leaf surface temperature and RH measured using four fabricated plant sensors, with each sensor being attached to the 9th leaf of a plant, and the standard deviation at five equally distributed time points per day over the 16-day measurement period. Figure 5b gives the mean value and standard deviation of the corresponding VPD calculated based on the measured temperature and RH. Overall, both the leaf RH and temperature exhibited expected diurnal changes during daytime and nighttime. The leaf temperature increased during daytime and decreased during nighttime, following the trend of changing the air temperature; however, the leaf surface generally exhibited a lower temperature than the air as expected due to the cooling effect of transpiration. The air temperature (obtained from the control system of the greenhouse) rose at daytime and dropped at night-time, while the air RH changed in an opposite direction. On the other hand, the leaf surface presented high RH in the day and low RH at night, acting in an opposite direction to the air RH. As the leaf RH was found generally higher than the air RH, indicating that the low moisture level in the air served as the driving force to evaporate water from the leaf.

Figure 6 depicts how light and irrigation affect the leaf RH, temperature, and VPD based on monitoring four maize plants grown under the same condition, where each plant had one sensor installed on the 9th leaf. As the light source of the greenhouse was switched off at 9 p.m., the average leaf RH was found to drop from ≈62% to ≈55% in ≈1 h, indicating the closure of stomata at low light. The leaf presented a temperature drop due to the cold air in the greenhouse. During the light-off time interval, while the overall RH went to a lower level, there were slight bumps of RH level that rose and fell, because the maize plant could open the stomata to accumulate carbon oxide and prepare for the photosynthesis during the light-on time. As the light source went back on at 6 a.m., the air temperature gradually increased to ≈30 °C, during which the average leaf RH gradually increased to ≈63%. The average leaf temperature was found to first increase to a level close to the air temperature and then dropped to ≈23 °C. The cooling down of the leaf may be associated with the leaving of water vapor from the leaf through transpiration. It should be pointed out that the average leaf temperature dropped at nighttime, indicating that the turning off of the greenhouse light (that were to lower the leaf temperature) could affect the leaf temperature more significantly than the closing of the stomata (that were to lift the leaf temperature). The average VPD was found to generally go lower than 1 kPa at night-time and rise above that at daytime (Figure 6b). Further, Figure 6c shows an example of using the sensors to monitor how the leaf RH and temperature would change with irrigation in the greenhouse obtained from four maize plants grown under the same condition. The irrigation was applied at 11:20 a.m., ≈1.5 h after the irrigation, there appeared an increase in average leaf RH from ≈48% to ≈65%. Figure 6d shows the dynamic change of average VPD obtained based on the measured leaf RH and temperature, indicating that the VPD dropped from ≈1.3 kPa and ≈0.4 kPa after the irrigation. In addition, a large drop of VPD was observed at 09:00 (Figure 6b) and at 19:00 (Figure 6d), which may be associated with the obvious leaf temperature drop at these two times (Figure 6a,c). Essentially, the decrease of leaf temperature may lead to a drop of saturated vapor pressure or VP_{sat} inside the leaf, which, in turn, reduces the VPD, according to the aforementioned VPD equation.

Essentially, the time from irrigating to clearly observing an increase in leaf RH indicates the time required for the plant to absorb and transport water from the root to the leaf where the sensor was installed. Therefore, by installing sensors at

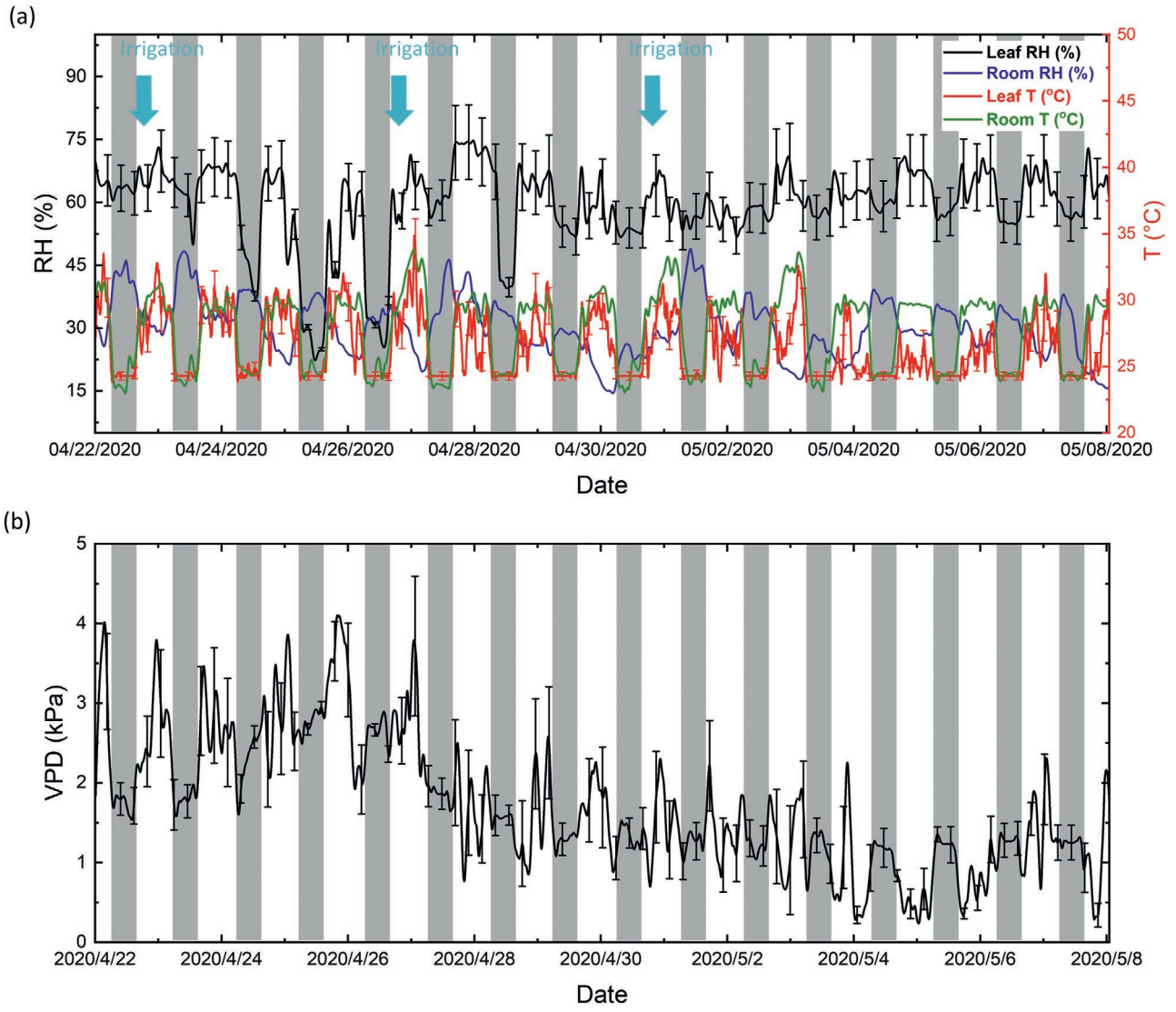

Figure 5. a) Mean leaf surface temperature and RH obtained from monitoring four maize plants with one sensor each at the 9th leaf; the error bars represent the standard deviation of the leaf temperature and RH measurements, and are given at five equally distributed time points per day. The air RH and temperature data were obtained from the greenhouse control system. b) Mean VPD calculated based on the measured temperature and RH given in (a). The error bars represent the standard deviation of the VPD. The plant sensors were installed ≈20 cm away from the stem at the back of the 9th leaf of four maize plants grown in the greenhouse under the same condition. The gray shadows specify the time when the light in the greenhouse was turned off.

different leaves, it is possible to estimate the time of water transport from proximal to distal leaves with respect to the root system. Further, when multiple sensors were attached in different areas of a leaf along the longitudinal direction toward the apex, the time required for water transport from one area to another in the leaf could be estimated. For example, two sensors were installed at the back of the lower (4th from the soil surface) leaf and the higher (9th) leaf, each being near the stem. The irrigation application was scheduled at 10:30 a.m. **Figure 7**a demonstrates that the lower and the higher leaf exhibited a distinct time difference in presenting a change in leaf RH. The RH level at the lower leaf increased from ≈40% to ≈67% in ≈30 min after the irrigation, while it took ≈3 h to initiate a RH rise on the higher leaf; therefore, there exhibited a time difference of 2.5 ± 0.6 hours (mean ± standard deviation; number of plants $n = 4$) between the two sensors presenting obvious RH signals. Interestingly, Figure 7b demonstrates that the sensor attached on the leaf at 10 cm to the stem exhibited a distinct RH change 0.5 ± 0.2 h (mean ± standard deviation; $n = 4$) earlier than that of the sensor installed 20 cm to the stem; this is reasonable as it took a longer time to transport water to the area on the leaf more distant from the stem.

Moreover, we conducted a pilot experiment in a maize plant field with the fabricated plant sensors. The sensors were deployed in a fertilized (168 kg N ha^{-1}) plot and an unfertilized one to examine the effect of the fertilization on the leaf RH and temperature of the plants. In each plot, four plants were randomly selected. Each sensor was placed on the same 4th leaf

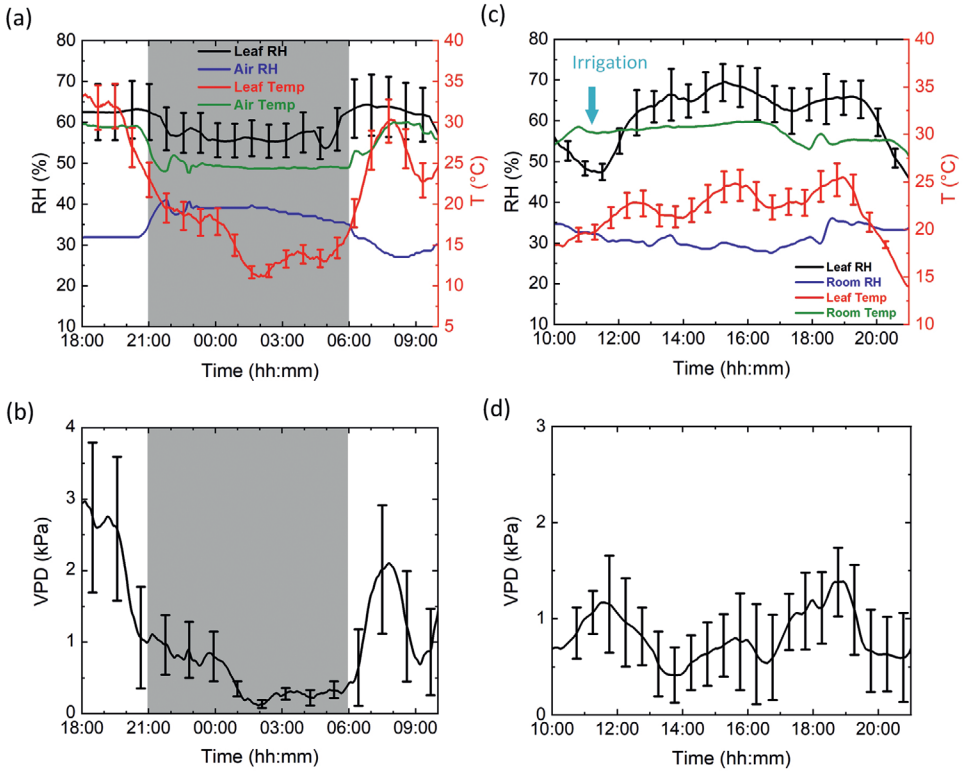

Figure 6. a,b) Mean leaf surface RH, temperature, and VPD of the plants in response to varying light condition and c,d) applying irrigation; the error bars in (a–d) represent the standard deviation and are given at 20 equally distributed time points; here, the statistical analysis was performed based on the data obtained from monitoring four maize plants grown under the same condition. Each sensor was installed ≈20 cm away from the stem at the back of the 9th leaf of the plant. The air RH and temperature data were obtained from the greenhouse control system. The grey shadows in (a) and (c) specify the time when the light in the greenhouse was turned off.

and 10 cm to the stem of plant. Data loggers were placed in waterproof containers for real-time data collection at a rate of 1 point per minute for 3 days. A statistical analysis was performed using the data obtained from monitoring four fertilized and four unfertilized plants.

Figure 8a shows the leaf surface temperature and RH of the fertilized and unfertilized plants measured using the fabricated plant sensors. The result shows that at nighttime, both the leaf and air RH rose to ≈100% while both the leaf and air temperature dropped. When the sun rose in the morning, the leaf and air RH decreased with increasing air temperature. With increasing photosynthesis at daytime, the leaves released more water vapor from the stomata, resulting in an increase in leaf RH to a level higher than the air RH. Figure 8b shows a close-up of the measurement result on the 4th of August, 2020. Compared to the unfertilized plants, the fertilized plants

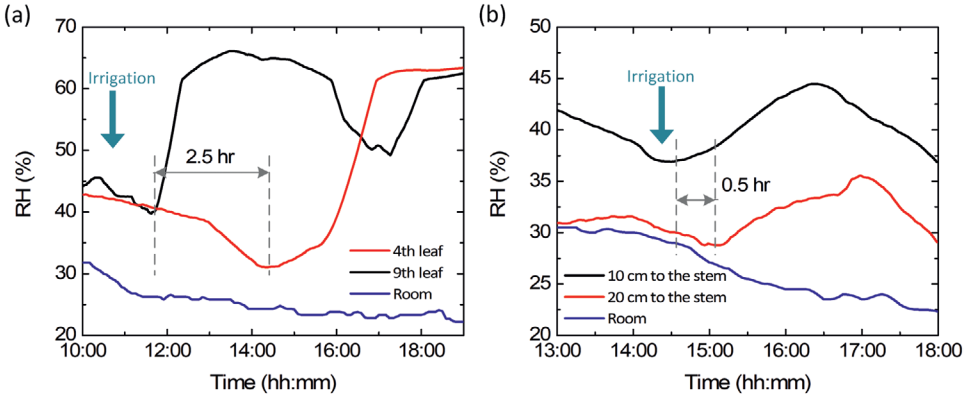

Figure 7. a) Dynamic RH changes at the lower (4th) and upper (9th) leaves of the plant upon the irrigation. The two sensors were installed ≈5 cm away from the stem. b) Dynamic RH changes in two areas on the 10th leaf. The two sensors used here were installed 10 and 20 cm, respectively, to the stem. The room RH data was obtained from the greenhouse control system.

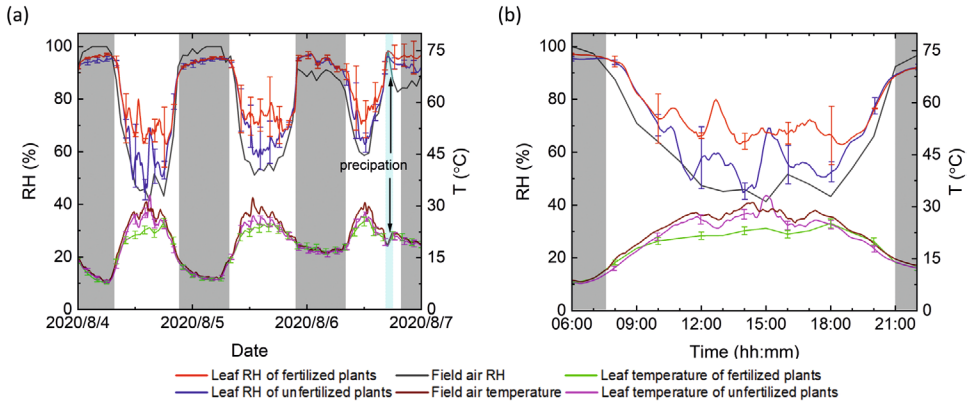

Figure 8. a) Mean leaf surface RH and temperature of the fertilized and unfertilized maize plants measured using the plant sensors under a field condition. The error bars represent the standard deviation of leaf surface RH and temperature from monitoring four fertilized and four unfertilized plants, and are given at 12 equally distributed time points per day over 3 days. b) Close-up of the measurement during the 4th of August, 2020. The gray shadows specify the time when the light in the greenhouse was turned off.

released more water vapor due to greater photosynthesis, thus presenting a higher RH and a lower temperature at the leaf; indeed, over the course of the growing season, the fertilized plants fixed ≈200% more carbon dioxide than the unfertilized plants which requires greater transpiration.

Field-deployable sensors are in great demand to provide accurate information on the crop development and growth status to optimize necessary agriculture management practices.[43,44] Potentially, the direct on-leaf measurements of the sensors will facilitate the development of new crop cultivars for improved water use, through characterizing the variations in transpiration of different cultivars. By integrating the presented plant sensor and our recently developed soil water potential sensor,[45] it is possible to create a sensors-based in-field water use monitoring platform to measure differences in water dynamics across a number of hybrids. There are phenotypic variations for water use among different hybrids that can be harnessed to develop crop varieties that acquire more carbon dioxide and nutrients per unit of water lost through stomata.

4. Conclusions

Accurate and continuous VPD measurement is highly desired. Doing so, however, requires the ability to capture subtle changes in both temperature and RH at the leaf surface. We have demonstrated a wearable and flexible plant sensor capable of continuous monitoring of dynamic changes in RH and temperature on the leaf surface, to facilitate the accurate calculation of VPD. This sensor is realized by integrating the LIG-based RH sensing unit and the Au-based thin-film thermistor on a flexible polyimide sheet. The simultaneous measurements for both temperature and RH on the leaf allow precise determination of VPD of the plant. The 16-day continuous measurement of the sensor has demonstrated the durability of the sensor in the greenhouse. The sensor has further validated in providing the information on how the light illumination, irrigation, and fertilization on the transpiration of the plants. We have incorporated multiple sensors to estimate the time required for water movement from the roots to each of the measured leaves, from the lower to higher leaves, and from one area to another on the same leaf. Further, the pilot field experiment has showed that the sensors are able to describe the difference in transpiration of the fertilized from the unfertilized corn plants under the field condition. The fertilized plants were found to release more water vapor to the air due to their high-level photosynthesis and transpiration.

There is much room to improve the presented plant sensor. For example, it is possible to form a complete sensor-based monitoring system on the leaf by integrating the electronic readout circuit, wireless communication capability, and energy harvesting method on the same flexible substrate. It should be noted that while considerable wearable devices have been developed for human medical, healthcare, and wellness, sensing for crops are relatively under-research. We believe that this presented sensor will provide a new method toward digital agriculture for increasing water use of crop plants.

Acknowledgements

This work was supported in part by the United States Department of Agriculture-National Institute of Food and Agriculture under Grants 2018-67021-27845 and 2020-67021-31528, and in part by the Plant Sciences Institute at Iowa State University. The authors thank Yang Tian for depositing a thin-film gold layer with e-beam evaporation, Dr. Xinran Wang and Yuncong Chen for technical discussions, and Ms. Lisa Coffey for assistance with plant care.

Conflict of Interest

The authors declare no conflict of interest.

Data Availability Statement

The data that support the findings of this study are available from the corresponding author upon reasonable request.

Keywords

flexible sensors, graphene, in-field measurement, plant sensors, transpiration

Received: December 14, 2020
Revised: January 30, 2021
Published online:

[1] J. Urban, M. W. Ingwers, M. A. McGuire, R. O. Teskey, *J. Exp. Bot.* **2017**, *68*, 1757.
[2] H. Bauer, P. Ache, S. Lautner, J. Fromm, W. Hartung, K. A. S. Al-Rasheid, S. Sonnewald, U. Sonnewald, S. Kneitz, N. Lachmann, R. R. Mendel, F. Bittner, A. M. Hetherington, R. Hedrich, *Curr. Biol.* **2013**, *23*, 53.
[3] K. Raschke, W. F. Hanebuth, G. D. Farquhar, *Planta* **1978**, *139*, 73.
[4] Z. Xu, G. Zhou, H. Shimizu, *Plant Signaling Behav.* **2010**, *5*, 649.
[5] H. G. Jones, *J. Exp. Bot.* **1998**, *49*, 387.
[6] V. B. Koman, T. T. S. Lew, M. H. Wong, S. Y. Kwak, J. P. Giraldo, M. S. Strano, *Lab Chip* **2017**, *17*, 4015.
[7] A. L. Fletcher, T. R. Sinclair, L. H. Allen, *Environ. Exp. Bot.* **2007**, *61*, 145.
[8] E. H. Hogg, P. A. Hurdle, *Tree Physiol.* **1997**, *17*, 501.
[9] N. Katsoulas, A. Baille, C. Kittas, *Agric. For. Meteorol.* **2001**, *106*, 233.
[10] G. W. Koch, J. S. Amthor, M. L. Goulden, *Tree Physiol.* **1994**, *14*, 347.
[11] J. Lihavainen, V. Ahonen, S. Keski-Saari, A. Sõber, E. Oksanen, M. Keinänen, *Tree Physiol.* **2017**, *37*, 1166.
[12] F. Vurro, M. Janni, N. Coppedè, F. Gentile, R. Manfredi, M. Bettelli, A. Zappettini, *Sensors* **2019**, *19*, 4667.
[13] J. R. Millan-Almaraz, R. Romero-Troncoso, J. de, R. G. Guevara-Gonzalez, L. M. Contreras-Medina, R. V. Carrillo-Serrano, R. A. Osornio-Rios, C. Duarte-Galvan, M. A. Rios-Alcaraz, I. Torres-Pacheco, *Sensors* **2010**, *10*, 8316.
[14] J. C. Ramos-Fernández, J. F. Balmat, M. A. Márquez-Vera, F. Lafont, N. Pessel, E. S. Espinoza-Quesada, *IFAC-PapersOnLine* **2016**, *49*, 371.
[15] S. Oren, Z. Wang, X. Wang, S. Tabassum, Y. Jiao, B. J. Montgomery, N. Neihart, C. M. McNinch, P. S. Schnable, L. Dong, *IEEE Int. Conf. Nano/Micro Eng. Mol. Syst., 12th* **2017**, 402.
[16] D. Zhang, Q. Du, Z. Zhang, X. Jiao, X. Song, J. Li, *Sci. Rep.* **2017**, *7*, 43461.
[17] H. Jeong, L. Wang, T. Ha, R. Mitbander, X. Yang, Z. Dai, S. Qiao, L. Shen, N. Sun, N. Lu, *Adv. Mater. Technol.* **2019**, *4*, 1900117.
[18] J. U. Lee, Y. W. Ma, S. Y. Jeong, B. S. Shin, *Micromachines* **2020**, *5*, 476.
[19] D. H. Ho, Q. Sun, S. Y. Kim, J. T. Han, D. H. Kim, J. H. Cho, *Adv. Mater.* **2016**, *28*, 2601.
[20] R. Park, H. Kim, S. Lone, S. Jeon, Y. W. Kwon, B. Shin, S. W. Hong, *Sensors* **2018**, *18*, 1857.
[21] S. Karthick, H.-S. Lee, S.-J. Kwon, R. Natarajan, V. Saraswathy, *Sensors* **2016**, *16*, 2079.
[22] J. Cai, C. Lv, E. Aoyagi, S. Ogawa, A. Watanabe, *ACS Appl. Mater. Interfaces* **2018**, *10*, 23987.
[23] S. Oren, H. Ceylan, P. S. Schnable, L. Dong, *Adv. Mater. Technol.* **2017**, *2*, 1700223.
[24] L. Lan, X. Le, H. Dong, J. Xie, Y. Ying, J. Ping, *Biosens. Bioelectron.* **2020**, *165*, 112360.
[25] Y. Lu, K. Xu, L. Zhang, M. Deguchi, H. Shishido, T. Arie, R. Pan, A. Hayashi, L. Shen, S. Akita, K. Takei, *ACS Nano* **2020**, *14*, 10966.
[26] V. B. Koman, T. T. Lew, M. H. Wong, S. Y. Kwak, J. P. Giraldo, M. S. Strano, *Lab Chip* **2017**, *17*, 4015.
[27] H. Ibrahim, S. Moru, S. -M. Kang, S. Yin, Y. Chen, L. Dong, *IEEE Int. Conf. Nano/Micro Eng. Mol. Syst., 15th* **2020**, 571.
[28] Z. Li, R. Paul, T. B. Tis, A. C. Saville, J. C. Hansel, T. Yu, J. B. Ristaino, Q. Wei, *Nat. Plants* **2019**, *5*, 856.
[29] T. T. S. Lew, V. B. Koman, K. S. Silmore, J. S. Seo, P. Gordiichuk, S. Y. Kwak, M. Park, M. C. Y. Ang, D. T. Khong, M. A. Lee, M. B. Chan-Park, *Nat. Plants* **2020**, *6*, 404.
[30] S. Moru, H. Ibrahim, L. Dong, *IEEE Int. Conf. Nano/Micro Eng. Mol. Syst., 15th* **2020**, 565.
[31] Y. Jiao, X. Wang, Y. Chen, M. J. Castellano, J. C. Schnable, P. S. Schnable, L. Dong, *Int. Conf. Solid-State Sens., Actuators Microsyst. Eurosens., 20th* **2019**, 37.
[32] T. A. Howell, *ASCE J. Irrig. Drain. Eng.* **2015**, *121*, 9437.
[33] P. G. Su, C. F. Chiou, *Sens. Actuators, B* **2014**, *200*, 9.
[34] A. I. Oliva, J. M. Lugo, R. A. Gurubel-Gonzalez, R. J. Centeno, J. E. Corona, F. Avilés, *Thin Solid Films* **2017**, *623*, 84.
[35] S. P. Singh, Y. Li, A. Be'Er, Y. Oren, J. M. Tour, C. J. Arnusch, *ACS Appl. Mater. Interfaces* **2017**, *9*, 18238.
[36] F. Tehrani, B. Bavarian, *Sci. Rep.* **2016**, *6*, 27975.
[37] H. Zobeiri, R. Wang, Q. Zhang, G. Zhu, X. Wang, *Acta Mater.* **2019**, *175*, 222.
[38] H. Zobeiri, R. Wang, C. Deng, Q. Zhang, X. Wang, *J. Phys. Chem. C* **2019**, *123*, 23236.
[39] J. M. Tulliani, B. Inserra, D. Ziegler, *Micromachines* **2019**, *10*, 232.
[40] K. K. Adhikari, C. Wang, T. Qiang, Q. Wu, *Appl. Phys. Express* **2019**, *12*, 106501.
[41] J. Luo, Y. Yao, X. Duan, T. Liu, *J. Mater. Chem. C* **2018**, *6*, 4727.
[42] T. Nakajima, T. Nakamura, T. Tsuchiya, *RSC Adv.* **2016**, *6*, 95342.
[43] Z. Xu, X. Wang, R. J. Weber, R. Kumar, L. Dong, *IEEE Sens. J.* **2017**, *17*, 4330.
[44] M. A. Ali, W. Hong, S. Oren, Q. Wang, Y. Wang, H. Jiang, L. Dong, *Rsc Adv.* **2016**, *6*, 67184.
[45] Y. Chen, Y. Tian, X. Wang, L. Wei, L. Dong, *IEEE Sens. J.* **2020**, *20*, 14109.